Heliyon 5 (2019) e01579

Contents lists available at ScienceDirect

Heliyon

journal homepage: www.heliyon.com

Heliyon

Algorithmic analysis for dental caries detection using an adaptive neural network architecture

Shashikant Patil [a,*], Vaishali Kulkarni [b], Archana Bhise [b]

[a] SVKMs, NMIMS. MPSTME Mumbai, India
[b] EXTC Department, SVKMs, NMIMS, MPSTME, Mumbai, India

ARTICLE INFO

Keywords:
Health sciences
Mathematics
Computer science
Dentistry

ABSTRACT

Objectives: AI techniques have lifelong impact in biomedics and widely accepted outcomes. The sole objective of the study is to evaluate accurate detection of caries using feature extraction and classification of the dental images along with amalgamation Adaptive Dragonfly algorithm (DA) algorithm and Neural Network (NN) classifier.
Materials and methods: Here proposed caries detection model is designed for detecting the tooth cavities in an accurate manner. This methodology has two main phases; feature extraction and classification. In all total 120 images database is split into three sets, randomly for evaluating the performance. Further, this categorization of the test cases aids in ensuring the enhancement of the performance. In each of the test cases, there are 40 caries images the investigation in the performance of the proposed caries detection model was done in terms of accuracy, sensitivity, specificity, and precision, FPR, FNR, NPV, FDR, F1Score and MCC.
Results: Here MPCA with Nonlinear Programming and Adaptive DA, the proposed model is termed as MNP-ADA. The performance of the proposed MPCA-ADA model is evaluated by comparing it over the other existing feature extraction models. MPCA–ADA over the conventional classifier models like PCA-ADA, LDA-ADA and ICA-ADA in terms of performance parameters and MCC for all the test types and have superior results than the existing ones.
Conclusion: The research work emphasizes the prospective efficacy of IP and NN algorithms for the detection and diagnosis of dental caries. A novel and improved model shows substantially worthy performance in distinguishing dental caries using image processing techniques.

1. Introduction

In the recent times, the medical image processing provides various detection techniques for detecting the dental caries in an early stage [1]. The dental decay or tooth decay is generally referred to as dental caries, and this disease takes place in the hard tissue of the tooth due to the action of the micro-organisms. These dental cavities can be prevented at the individual level. In case, if the caries were not detected at the early stage, they may lead to more complex and may require costly treatments. This may also lead to huge infections on the pulp tissue inflammation [2, 3]. Hence, there is a necessity to detect the caries in an accurate way as well as in an early stage [18]. Since posterior teeth have larger proximal surfaces and mineral loss is insignificant in incipient caries, incipient approximal carious lesions in posterior teeth are often hard to detect. Thus, radiographic examination is extremely important for the evaluation of proximal surfaces of posterior teeth [4]. When the dental caries is larger in size, they can be viewed by naked eye, whereas, smaller lesions are difficult to identify. In the primary level of diagnosis, all the tooth surfaces of the patient are inspected by utilizing a light source, dental mirror and explorer [5, 6, 7]. Most of the diagnosis is made with the Dental radiographs (X-rays), and they are efficient in exhibiting the dental caries that takes place between the teeth [19, 20]. Further, the "hidden caries" are complex to estimate, because they are invisible at the surface [8]. These hidden caries are due to the bacterial action that penetrates the enamel in order to reach the inner surface of the teeth [21]. Here, the outer surface of the teeth will be intact. These types of hidden caries cannot be detected in an accurate way by using the X-rays [9, 10].

For the early diagnosis of tooth caries, more enhanced visual techniques were introduced. They made use of the light scattering phenomenon and is based on the depth of the wavelength of the light [15, 16]. It is capable of detecting the presence of absence of caries [11, 12]. But, this method requires different fluorescence of different colours. Then, the Ultrasound Caries Detector was used, in which the images of tissues can

* Corresponding author.
E-mail address: sspatil@ieee.org (S. Patil).

https://doi.org/10.1016/j.heliyon.2019.e01579
Received 10 January 2019; Received in revised form 13 March 2019; Accepted 24 April 2019

Table 1
Review of conventional classifiers.

Sl.No.	Author [Citation]	Methodology	Features	Challenges
1	Angelino *et al.* [1]	Near-Infrared Imaging (NIR)	• Simple to use. • Capacity to use multiple view angles.	• Transparency is not available • Not accurate
2	Keem And Elbaum [2]	Wavelet Transformation Method (WT)	• Higher sensitivity in detecting the caries at early lesion. • Absence of ionizing radiation.	• Not flexible • Contrast of the image is low
3	Rad *et al.* [3]	Neural Network (NN)	• Most suitable initial contour (IC) are formed. • Accurate and efficient in detection	• Requires vast computation • Setting of parameters are complex
4	Choi et al. [4]	FCNN	• Lack of redundancy problem. • Segmentation of crowns is achieved by level set method	• Noise is high • Data sets are insignificant
5	Kositbowornchai et al. [5]	ANN	• More stabile • High sensitivity and specificity	• Less diagnostic value • Training data cannot be used in addition.

be collected by reflected sound waves. This method reduced the amount of ionizing radiation and hence the caries detection was accurate [13, 14]. Even though most of the existing works on the classification of the caries region from the non decay region employs the dental explorer as well as X-ray radiography, these methods are found to be more complex [17]. Hence, there is a necessity to have an algorithmic analysis on the dental caries detection [23].

The main focus of this research is to propose a caries detection methodology on the basis of MPCA based feature extraction. The classification of the extracted features is accomplished using NN classifier. Once the features are extracted, they are multiplied with a weighting factor. Further, the Nonlinear Programming Optimization is employed with an intention of maximizing the distance between the resultant feature outputs. NN classifier is trained using an adaptive DA algorithm. An algorithmic analysis is carried out in this paper, by comparing the proposed MPCA-ADA model with other existing methods like PCA, LDA, ICA and MPCA in terms of accuracy, specificity, sensitivity, precision, False positive rate (FPR), False negative rate (FNR), Negative Predictive Value (NPV), False Discovery Rate (FDR), F1Score and Mathews correlation coefficient (MCC).

The rest of the paper is organized as follows: Section 2 reviews the literature work; Section 3 portrays the steps allotted for caries detection. Section 4 describes the architecture of proposed caries detection model. V discusses the obtained results, and Section 6 concludes the paper.

2. Background

2.1. Related works

As per tabulated in Table 1 many researchers contributed their valuable insights in the field of dental caries detection using image processing tools likewise in 2017, Angelino *et al.* [1] proffered NIR (850 nm) LED imaging system by interlinking NIR source as well as intraoral camera in order to evaluate the low sensitivity regions of the teeth. There is non-ionizing and safe approach in the range of NIR, while detecting the translucency of the teeth. Further, to obtain the caries in the ten consenting human subjects, the image of the teeth was provided by NIR and this NIR was responsible for providing the supplementary evaluations. Further, the de-mineralized areas were revealed along with the deep and superficial cracks by means of the camera-wand system. This method had high clinical utility, simple to use, user-friendly, and it was low in cost, while compared to the radiographs.

In 2007, Keem and Elbaum [2] formulated a new technique with the desire of processing the Digital Imaging Fiber-Optic Trans-illumination Images and recording the changes in the image (DIFOTI) that were obtained at distinct times. The three major contribution of this research were (a) segmentation of the teeth on the basis of wavelet modulus maxima. (b) Estimation of the location of caries tooth and its orientation by utilizing first and second moments of DIFOTO gray level. (c) Quantitative monitoring by multi-resolution wavelet magnitude representation.

In 2018, Rad *et al.* [3] formulated a novel segmentation method on the basis of Level Set (LS). The proposed model detected the tooth caries in two phases: generation of the morphological information of the dental image by means of utilizing the generated IC and by using the motion filtering as well as the back propagation neural network, the segmentation of the intelligent level set was made. The outcomes of the segmentation procedure were found to be much accurate while compared to the outcomes of the other caries detection method. Further, the feature map and the integral projection technique were employed with an intention of isolating the caries tooth from the other good tooth. The feature map was better in obtaining the caries area from the other area.

In 2018, Choi *et al.* [4] formulated automatic detection system with aspire of detecting the caries tooth in an early stage. In the proposed model, four modules were employed, such as horizontal alignment of pictured teeth, probability map generation, crown extraction, and refinement. Further, to enhance the performance of the proposed model, the pictured teeth were aligned in a horizontal manner. The probability map of the caries was generated from the fully convolutional network. The caries in the crown region were obtained from the optimization schemes as well as from the edge-based level set method. Moreover, in order to enhance the performance of detection, the non-maximum suppression method was indulged.

In 2006, Kositbowornchai *et al.* [5] formulated a novel neural network with an aim of detecting the artificial dental caries from the tooth by means of employing Charged-Coupled Device (CCD) camera and intra-oral digital radiography. In this method, the depth of the dental caries was evaluated using Graphic User Interface (GUI) that was developed on the MATLAB program. Further, the region of caries was discriminated from the other region by means of sound, and this is accomplished by the Learning Vector Quantization (LVQ) method. The diagnostic test was undergone in order to securitize the performance of the proposed model.

3. Design

3.1. Pre-processing

Three consecutive steps are followed in order to enhance the input image A.These stages are Contrast enhancement, Gray thresholding and Active contour.

3.1.1. Contrast enhancement

The resized image is represented as $A^B$and the enhancement of A^B takes place in this stage. In order to enhance the visibility of image, adjustments are made in the intensity of the image [29]. In this method, the visibility of image is improved with consideration in the values of the

relative darkness, and on the values of the brightness of A^B. The mathematical equation for contrast enhancement of image is represeneted in Eq. (1) in which A^B_{new} represents the contrast enhanced image. By means of enhancing the contrast of the image, A^B gets transformed into a grey level image and the newly formed grey level image is represented as A^B_{new}. Where, In_{low} and In_{high} indicate the contrast limits for the input image and Op_{high} and Op_{low} are the contrast limits for the output image.

$$A^B_{new} = \left(\begin{pmatrix} ((A^B - In_{low})/(In_{high} - In_{low}))\hat{\lambda} \\ * \\ (Op_{high} - Op_{low}) \end{pmatrix} \right) + In_{low} \quad (1)$$

3.1.2. Gray thresholding

The Otsu's thresholding [26] is utilized as a gray thresholding processing method in this paper. With respect to the position of the gray intensity, this processing method integrates any one of pixels (i.e., either black or white) [22]. Further, the transformation from white pixel to black pixel takes place when the image intensity A_p is found to be much smaller than the value of constant D^* i.e., $(A_p < D^*)$.

3.1.3. Active contour

By means of initializing a set of coordinates that are available in the image, there occurs generation of a contour or mask of the objective. Further, by the driven forces of image, there occurs reposition of the generated contour on the image. This reposition helps in generating borders to the specific objective. Two distinct kinds of driven forces are employed; they are internal energy and external energy [27]. The internal forces help in smoothening this mode, whereas, the external forces relocate the model. Hence, the generation contour is assisted by the set of coordinates. The mathematical equation for the set of coordinates is represented in Eq. (2) in which $G(u)$ signifies the set of coordinates and $u$represents the contour's normalized index of control point. Further, the coordinates of the contour are described as(x, y). Also, a set of coordinates $x(u)$and $y(u)$are used to create contour$G(u)$. Eq. (3) represents the aggregate energy of deformation model in which the curves interior energy forces and the exterior restriction are represented as$E^{(\mathrm{int})}$and$E^{(ext)}$, respectively. The energy image is denoted as$E^{(image)}$. The addition of elastic energy $E^{(elastic)}$with the bending energy $E^{(bend)}$paves way to the formation of internal energy and the control points' normalized index is represented as$u$. Eq. (4) represents the mathematical equation of internal energy$E^{(\mathrm{int})}$. The$\gamma(u)$ represents the adjustable constant which specifies the continuity, $\psi(u)$represents the adjustable constant that specifies contour curving.

$$G(u) = (x(u)y(u)); G(u) \in A^B_{new}(x, y) \quad (2)$$

$$E^{'} = \int_0^1 (E^{(\mathrm{int})a} G(u) + E^{(image)} G(u) + E^{(ext)} G(u))du \quad (3)$$

$$E^{(\mathrm{int})} = E^{(elastic)} + E^{(bend)} = \gamma(u)\left|\frac{dv}{du}\right|^2 + \psi(u)\left|\frac{d^2v}{du^2}\right|^2 \quad (4)$$

$$E^{(elastic)} = \gamma(G(u) - G(u-1))^2 du \quad (5)$$

$$E^{(bend)} = \psi(G(u-1) - G(u) + (G(u+1))^2 du \quad (6)$$

Further, from the active contour model, $A_m$represents the consequential pre-processed image.

3.2. Feature extraction

MPCA is utilized for extracting the features of the imageA_m. While comparing PCA with MPCA, better generation ability is found with MPCA during the image construction phase [28]. The rearrangement of the image into the 3D tensor is constructed using MPCA model and this rearranged is represented as $A_x \in R^{A^1_m \times A^2_m \times A^3_m}$in which the height and width of the image is represented as A^1_mandA^2_m, respectively. Further, A^3_mspecifies the ` count of images. The algorithm is summarized as follows:

(i) The mean of the matrix is computed as $\overline{N} = (1/A^3_m)\sum_{c=1}^{A^3_m} \overline{S}_c$

(ii) The tensor $\overline{A}_x$is centred as $\overline{A}_x = [\overline{S}_1 - \overline{N}, \overline{S}_2 - \overline{N}, ..., \overline{S}_{A^3_m} - \overline{N}]$

(iii) Within the matrix, $\overline{A}_x$is unfolded. In the unfolded matrix, the elements that are present in$h$mode are represented as$\overline{A}\begin{pmatrix} (h) \\ x \end{pmatrix}_{(index)} = y_{c_1 c_2 c_3}$, where index $= c_h$, $\sum_{g=3}^{h+1}(c_g - 1) + \sum_{g=h-1}(c_g - 1)$

(iv) The covariance matrix is utilized for the determination of the eigenvectors with the help of the Fmatrix in $h$mode, $D^{(h)} = F^*_{(h)} F^{*F}_{(h)}$. Further, the selected eigenvectors be $J_{(h)} = [J_1, J_2, ...J_{o_{(h)}}]$ and largest eigenvectors is represented as$O_{(h)}$.

(v) The feature selection is made in two types, they are (a) for varying modes $W_{c(h)} = (\overline{S}_c - \overline{N}) \times J^m_{(h)}$ is sampled and the extracted features are represented as $l = O_{(1)} \times A^2_m + O_{(2)} \times A^1_m$ (b) by$W_c = J^m_1(\overline{S}_c - \overline{N})J_{(2)}$ and here the extracted feature is specified as$l = O_{(1)} \times O_{(2)}$. It is vivid that, the features extracted from these two approaches are not similar.

(vi) By utilizing either of the feature sets, the process of classification can be undergone.

3.3. Classification phase

Feed forward NN classifier is utilized in various applications due to its flexibility over the other existing classifiers [25, 30]. The input to the NN is the chosen features that were obtained by multiplying the features with weights and this is done with an intention of recognizing the tooth caries. The obtained feature set $l^{(weight)}$is the input. Further, Eq. (7), Eq. (8) and Eq. (9) represent the network model of NN. In the network model, the hidden neuron is represented as $k$and the bias weight of the k^{th}neuron is specified as $wt^Q_{(hk)}$. The count of the input and the hidden neurons are denoted as $y^Z$and y^Q, respectively. Then, for thet^{th}-layer, the output bias weight is represnted as $wt^I_{(ht)}$. The weight of the input neuron from j^{th}layer to the hidden neuron ink^{th}layer is denoted as $wt^Q_{(jk)}$. Similarly, $wt^I_{(kt)}$denotes the output weight fromk^{th}layer of hidden neuron tok^{th}layer. Further, Eq. (8) manifests the network output and it is represented asX', whereas the actual output is represented as X. It is illustrated in Fig. 1. The output of NN provides the classified output image and from the image, the caries affected regions are distinguished from the other region. The error function is repressed as wt^*in Eq. (9), and it is the difference between the actual $X$and the predicted outputX'. The activation function is specified as FN. The input vector dimension allocated is 100, and the hidden layer used here is 1 and the hidden neurons are 10.

$$X = FN\left(wt^Q_{(hk)} + \sum_{s=1}^{y^Z} w^Q_{(jk)} l^{weight}\right) \quad (7)$$

$$X' = FN\left(wt^I_{(ht)} + \sum_{k=1}^{y^Q} wt^I_{(kq)} l^{weight}\right) \quad (8)$$

$$wt^* = \underset{\left\{wt^Q_{(hk)}, wt^Q_{(jk)}, wt^I_{(ht)}, wt^I_{(kq)}\right\}}{\operatorname{argmin}} \sum_{t=1}^{y^J} |X - X'| \quad (9)$$

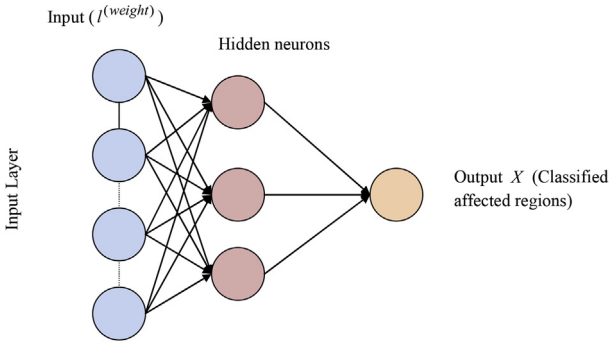

Fig. 1. Layout of feed forward neural natwork

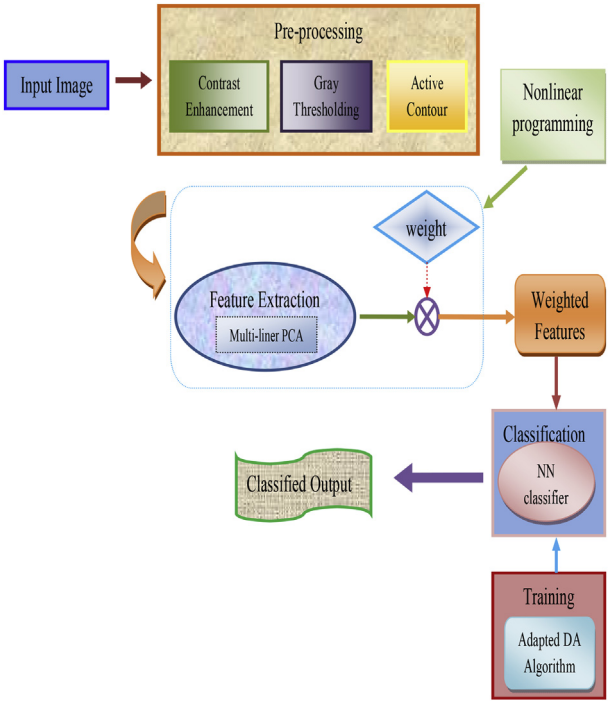

Fig. 2. Diagrammatic representation of proposed MPCA-ADA model for Caries Detection.

4. Methodology

4.1. Proposed archetype

Fig. 2 manifests the proposed dental caries recognition model. The proposed model indulges three phases:

(i) Pre-processing phase: This is the initial stage of caries detection. In this stage the input image is assumed as *A*and it is pre-processed by using three steps, they are contrast enhancement, grey thresholding, and active contour. After undergoing these three steps, the processed image $A_m$is obtained.

(ii) Feature Extraction phase: With an intention of extracting the features from the processed image, this paper makes use of MPCA. Further, to enhance the performance of diagnosis, the extracted features are multiplied with the weight that same size as that of the features. Then, among the obtained features$l^{(weight)}$, the distance between the features is maximized by means of employing the Nonlinear programming optimization method. The features obtained from this method are given to the classification phase

(iii) Classification phase: In order to classify the image and to predict whether the feature extracted image is normal or affected by cavity. Further, with the desire of classifying the non-caries and caries images, NN classifier is adopted in this research. The training of NN is accomplished by Adaptive Dragonfly optimization (ADA). Hence, the error between predicted and target values are diminished.

Further, with aspire of enhancing the performance of the proposed diagnosis method, the extracted features are multiplied with the weight and they are represented in Eq. (10) and Eq. (11), where, l and Wt are the extracted features and the weights, respectively. The weight ranges from 0 to 1. Further, there is a limitation that the size of obtained feature needs to be equal to the size of weight. Further, Eq. (12) represents the distance$Z_g$in between the obtained features$l^{(weight)}$. The distance between the features is maximized by using the Nonlinear programming optimization method. Further, Nonlinear programming optimization model is utilized for distance$Z_g$in which$g = 1, ...U_Z$. Further, Eq. (13) specifies the mathematical model of the objective function, in which the total count of the obtained features are represented as U_Z.

$$l = [l_1, ...l_{U_Z}] \tag{10}$$

$$Wt = [Wt_1, ...Wt_{U_Z}] \tag{11}$$

$$l^{weight} = l \times Wt \\ = l_1^{(weight)}, ...l_{U_Z}^{(weight)} \tag{12}$$

$$Obj = \max(Z_g); g = 1, 2.....U_Z \tag{13}$$

4.2. Non-linear programming optimization

Once the features are extracted, they are multiplied with a weighting factor ranges between [0,1], and the distance between the resultant feature outputs is maximized by employing Nonlinear Programming Optimization. If the distance between the selected features is high, it will obviously improve the classification performance as each feature provides unique information [29]. Eq. (14) manifests the problem that takes place under the nonlinear program. In Eq. (14), the differential functions are represented as$f'(n')$,$q'(n')$ and$o'(n')$. Further, Eq. (16) represents the series of barrier subproblems that are obtained from the interior function and hence the Eq. (14) gets altered as per Eq. (16). The vector of the stack variables is represented as$b' > 0$. The barrier parameters are represented as

$$d' = (n', b') \text{ and } \alpha > 0$$

$$\min_{n'} f'(n') = 0 \tag{14}$$

$$\text{Hence, } q'(n') = 0 \\ o'(n') = 0 \tag{15}$$

$$\min_{d'} \rho_\alpha(d') \equiv f'(n') - \alpha \sum_{z'}^{y'} Int \ \ b'_{z'} \tag{16}$$

$$\text{Hence, } q'(n') = 0 \\ o'(n') + b' = 0 \tag{17}$$

Further, Eq. (18) represents the Lagrangian function that is related to Eq. (16). In Eq. (18), the lagrange multipliers are represented as $\phi_{q'}, \phi_{i'}$ and $\phi = (\phi_{q'}, \phi_{i'})$.

$$\aleph(d', \varphi;) = \varphi_\mu(\widehat{k}) + \alpha_{q'}^{M'} q'(n') + \alpha_{i'}^{M'} (i'(n') + b') \tag{18}$$

Further, Eq. (19) represents the first order optimality conditions that

were related to the barrier issue as per Eq. (16). In Eq. (19), the diagonal matrices are described as $V'$and $\Gamma_{\hat{i}}$ and the Jacobian matrices are specified as $M'_{q'}$and $M'_{\hat{i}}$. Further, the values of $b'$and $\varphi_{\hat{i}}$are said to have a non-negative value.

$$\begin{bmatrix} \nabla f'(n') + M'_{q'}(n')^{Y'}\phi_{q'} + M'_{\hat{i}}(n')^{Y'}\phi_{\hat{i}} \\ V'\Gamma_{\hat{i}}w' - \alpha w' \end{bmatrix} = \begin{bmatrix} 0 \\ 0 \end{bmatrix} \tag{19}$$

Then, a primal dual system is formed, while applying newton's method to the current iteration $(d', \phi)$and it is represented in Eq, (20).

$$\text{where, } L'_{d'} = \begin{bmatrix} L'_{n'} \\ L'_{b'} \end{bmatrix}, L'_{\phi} = \begin{bmatrix} L'_{q'} \\ L'_{\hat{i}'} \end{bmatrix}, C'(d') = \begin{bmatrix} q'(n') \\ o'(n') + b' \end{bmatrix}, M'(n') = \begin{bmatrix} M'_{q'}(n')o \\ M'_{\hat{i}}(n')1 \end{bmatrix} \text{and } G'(d', \phi; \alpha) = \begin{bmatrix} \nabla^2_{n'n'}\aleph(d', \phi; \alpha) & 0 \\ 0 & V'^{-1}\Gamma_{\hat{i}'} \end{bmatrix}$$

$$\begin{bmatrix} G'(d', \phi; \alpha) & M'(n')^{Y'} \\ M'(n') & 0 \end{bmatrix} \begin{bmatrix} L'_{d'} \\ L'_{\phi} \end{bmatrix} = -\begin{bmatrix} \nabla_{d'}\aleph(d', \phi; \alpha) \\ c'(d') \end{bmatrix} \tag{20}$$

$$d'^{+} = d' + \tau_{d'}L'_{d'}, \ \phi^{+} = \phi + \tau_{\phi}L'_{\phi} \tag{21}$$

$$\begin{aligned} \tau^{\max}_{d'} &= \max[\tau \in (0,1)] : \hat{l} + \tau L'_{b'} \geq (1-\delta)b' \\ \tau^{\max}_{\phi} &= \max[\tau \in (0,1)] : \phi_{\hat{i}} + \tau L'_{\hat{i}'} \geq (1-\delta)\phi_{\hat{i}} \end{aligned} \tag{22}$$

Further. Eq. (21) represents the new iteration and the step length is represented as $\tau_{d'}$ andτ_{ϕ}. Then, as per Eq. (22), in order to two stages are required for formulating the step-lengths.

4.3. Adaptive Dragonfly optimization

The training of NN classifier is done by using ADA, which is a modified version of DA. The network keeps training all the patterns repeatedly until the total error falls to some pre-determined low target value and then it stops. When the network has fully trained, the Validation Set error reaches a minimum. Here, 75% of data is used for training and 25% data is used for testing. Survival is the main objective of each group, and hence the individual dragonfly are attracted towards the food and distracted away from the external enemies. Further, on the basis of these two behaviours, five factors were generation in order to update the location of each individual dragonfly [24]. The five factors are (i) Control cohesion (ii) Alignment (iii) Separation (iv) Attraction (v) Distraction. Eq. (23) represents the separation of r^{th}dragonfly and this separation is represented as B_r. Further, the position of present dragonfly and the location of z^{th} neighboring dragonfly are represented $\widehat{V}$and$\widehat{V}_{\widehat{z}}$, respectively, and the count of the neighboring dragonflies are represented as$\widehat{M}$. Further, as per Eq. (24), the alignment is evaluated and in this equation velocity ofs^{th}neighboring dragonfly is represented as$F^*_{\widehat{z}}$. Then, the assessment of the cohesion is done as per Eq. (25). The dragonfly gets attracted towards the food, and this attraction movement is represented in Eq. (25). Further, the dragonfly gets distracted while there is an enemy and this represented in Eq. (26). In these equations, the food source and the external enemy is specified as FSandEE, respectively.

$$B_r = \sum_{f=1}^{\widehat{M}} \left(\widehat{V} - \widehat{V}_{\widehat{z}}\right) \tag{23}$$

$$\widehat{J}_r = \frac{\sum_{z=1}^{\widehat{M}} F^*_{\widehat{z}}}{\widehat{M}} \tag{24}$$

$$\widehat{I}_r = \frac{\sum_{z=1}^{\widehat{M}} \widehat{V}_{\widehat{z}}}{\widehat{M}} - \widehat{V} \tag{25}$$

$$\widehat{N}_r = FS - \widehat{V} \tag{26}$$

$$\widehat{T}_r = EE + \widehat{V} \tag{27}$$

The five patterns that are already mentioned portray the behaviour of dragonflies. Then, with the desire of renewing the position of the dragonflies, the step vector $\Delta\widehat{V}$ and position vectors $\widehat{V}$are utilized. The dragonfly algorithm is related to Particle Swarm Optimization (PSO) algorithm, since the step vector$\Delta\widehat{V}$ of dragonfly algorithm is equal to the PSO's velocity vector. Further, in order to represent the direction in which the dragonflies are migrating, step vector $\Delta\widehat{V}$is used, and this is shown in Eq. (28). Here, separation weight is described as $\hat{n}$, the separation of r^{th}dragonfly is represented as $B_r$and the alignment weight is denoted as $\hat{y}$. Further, the alignment of r^{th}dragonfly is denoted as J_r, and$\hat{m}$ represents the cohesion weight. In addition to this, the cohesion of r^{th} dragonfly is specified as $\widehat{I}_r$,and the food source, enemy factor and position of enemy of r^{th} dragonfly are represented as $\widehat{N}_r$,$\widehat{t}$and$\widehat{T}_r$, respectively. The internal weight of the dragonfly and the iteration counter is denoted as $\xi$and $\widehat{i}$, respectively. By means of optimizing these factors, then exploitative as well as explorative behaviors of the dragonfly can be secruntized. Further, the dragons position vector is determined as shown in Eq. (29), in which the present iteration is represented as $\widehat{i}$,and the local and the global best solutions are represented as $\widehat{O}^{best}$and $\widehat{R}^{best}$, respectively.

$$\Delta\widehat{V}_{\widehat{i+1}} = \left(\hat{n}\widehat{B}_r + \hat{y}J_r + \hat{m}\widehat{I}_r + \hat{q}\widehat{N}_r + \widehat{d}\widehat{T}_r\right) + Wr.\Delta\widehat{V}_{\widehat{i}} \tag{28}$$

$$\widehat{V}_{\widehat{i+1}} = \widehat{V}_{\widehat{i}} + \Delta\widehat{V}_{\widehat{i+1}} + \left(\widehat{O}^{best} + \widehat{R}^{best}\right) \times \omega \tag{29}$$

$$\omega = \frac{\widehat{V}\left(\widehat{i}-1\right) - \widehat{V}\left(\widehat{i}\right)}{\widehat{V}\left(\widehat{i}\right)} \tag{30}$$

At the time of exploration of the search space, an assumption is made with the dragonfly with great alignment and less cohesion, whereas, less alignment and great cohesion are assigned to the dragonflies during the exploitation phase. Further, in the absence of the neighborhood solutions, a random walk is made by the dragonflies in terms of randomness, exploration and stochastic behavior. In the random walk stage, the position of the dragonflies is renewed by utilizing Eq. (31), in which the current iteration and the dimensions of position vectors are represented as $\widehat{i}$and$\widehat{d}$, respectively. Moreover, in the interval [0,1], the two random numbers are denoted as $\widehat{g}_1$and $\widehat{g}_2$,and the inertial weight is represented as Wr. Then, the updating of the dragonflies takes place, while increasing the iteration and this updating is done using the mathematical equations Eq. (28), Eq. (29) and Eq. (31). By means of equating the Euclidean distance in the whole dragonfly with optimal$\widehat{M}$, it is possible to predict the neighbour of each and every individual dragonfly. Once the neighbours are defined,$\widehat{V}$and $\Delta\widehat{V}$are renewed. Moreover, until the last criterion gets satisfied, the updating of the position takes place. At the end of the training process, an optimal weight will be produced by the algorithm, which in turn is multiplied with the extracted features obtained from the classifier.

$$\widehat{V}_{\widehat{i+1}} = \widehat{V}_{\widehat{i}} + lev\left(\widehat{f}\right) \times \widehat{V}_{\widehat{i}} \tag{31}$$

$$lev\left(\widehat{f}\right) = 0.01 \times \frac{\widehat{g}_1 \times \vartheta}{\left|\widehat{g}_2\right|^{\frac{1}{\widehat{f}}}} \tag{32}$$

$$\vartheta = \left(\frac{\varepsilon(1+\xi) \times \sin\left(\frac{\pi\xi}{2}\right)}{\sigma\left(\frac{1+\xi}{2}\right) \times \xi \times 2^{\left(\frac{\xi-1}{2}\right)}}\right) \tag{33}$$

$$\sigma(\widehat{p}) = (\widehat{p}-1)!$$

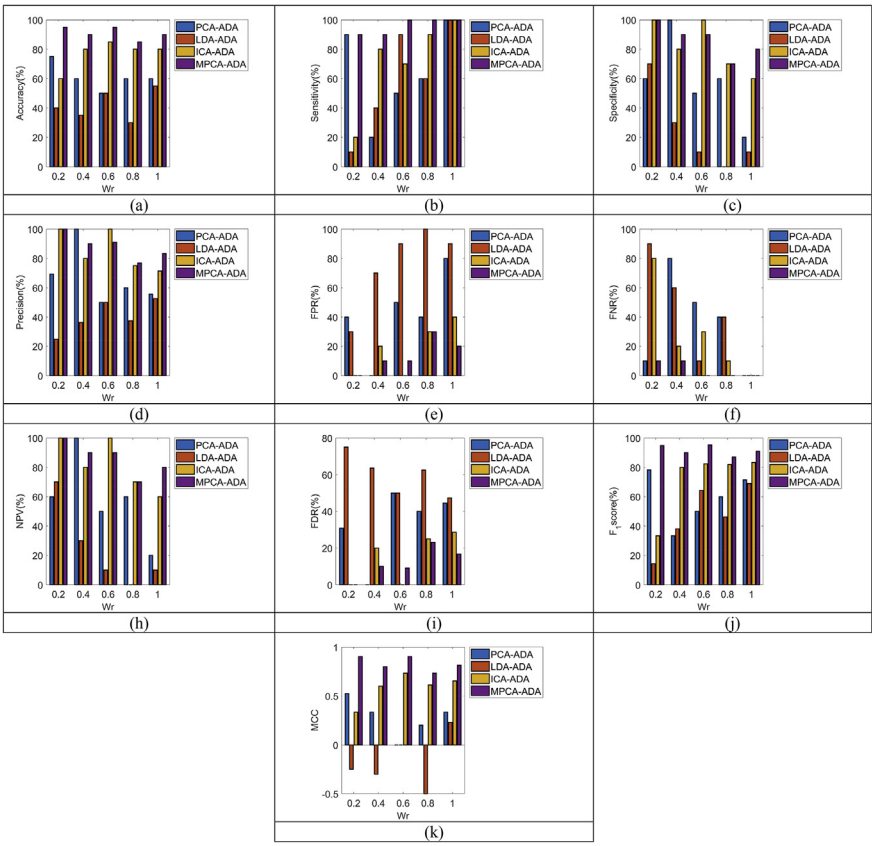

Fig. 3. Algorithmic analysis on the performace of proposed MPCA-ADA over the existing classifier for Test Case 1 in terms of (a) Accuracy (b) Sensitivity (c) Specificity (d)Precision (e) FPR (e) FPR (f) FNR (g) NPV (h) FDR (i) F1- score (j) MCC.

5. Results and discussion

5.1. Experimental setup

MATLAB 2015a is utilized as tool for conducting the experimental evaluations on the dental caries detection. The database for this evaluation was obtained from (https://mynotebook.labarchives.com/share/Vahab/MjAuOHw4NTc2Mi8xNi9UcmVlTm9kZS83NzM5OTk2MDZ8NTIuOA: Access date 11-12-2018). The images collected for this study are 120 periodical digital dental X-ray images in which the abnormality of each images has been specified by dental experts. All images are gray scale digitized X-ray with a dimension of 748×512 where the last 12 rows contain the information of images and must be removed in the analyzing process. Regularly, each image contains at least one to four complete teeth. The images are digitized in the format of ''jpeg'' file type, which is a popular image type in image processing. Images are evaluated by the experts to ensure that all the images are suitable for the analysis process. The image acquisition process downloaded database is split into three sets, viz., test case 1, test case 2 and test case 3 randomly for evaluating the performance. Further, this categorization of the test cases aids in ensuring the enhancement of the performance. In each of the test cases, there are 40 caries images. Moreover, the investigation in the performance of the proposed caries detection model was done in terms of accuracy, sensitivity, specificity, precision, FPR, FNR, NPV, FDR, F_1Score and MCC.

5.2. Algorithmic analysis for test case 1

Fig. 3 summarizes the performance analysis of proposed MPCA-ADA classifier over the other conventional classifiers by varying the weight factor *Wr* (Eq. (28)) under test case 1. From Fig. 2(a), the accuracy of the proposed MPCA-ADA is found to be 20%, 55%, and 33% better than PCA-ADA, LDA-ADA and ICA-ADA, respectively, at$Wr = 0.2$. Then, at $Wr = 0.6$ in Fig. 2(b), the sensitivity of the proposed MPCA-ADA model is 60%, 40% and 33% superior to the traditional models like PCA-ADA, LDA-ADA, and ICA-ADA, respectively. The developed MPCA-ADA is enhanced over the state-of-art models like PCA-ADA by 75%, LDA-ADA by 87% and ICA-ADA by 25% in terms of specificity, at$Wr = 1$ as per Fig. 2(c). Then, from Fig. 2(d), at $Wr = 1$ the precision of the proposed MPCA-ADA model is securitized as 60%, 77% and 23% better than the existing models like PCA-ADA, LDA-ADA and ICA-ADA, respectively. From Fig.2 (e), it is clear that the proposed MPCA-ADA model is 75% better than PCA-ADA, 76.4% better than LDA-ADA and 50% better than ICA-ADA with minimum FPR at$Wr = 1$. Similarly at$Wr = 0.6$, the proposed MPCA-ADA model is evaluated to be 88%, 66%, 83% better than the traditional models like PCA-ADA, LDA-ADA and ICA-ADA, respectively in terms of minimal FNR as per Fig. 2(f). The NPV at $Wr = 1$for the proposed MPCA-ADA model is 75%, 33% and 25% superior to the conventional models like PCA-ADA, LDA-ADA and ICA-ADA, respectively as shown in Fig. 2(g). Further, from Fig.2 (h), the proposed MPCA-ADA model is 75%, 33% and 25% superior to the traditional models like PCA-ADA, LDA-ADA, ICA-ADA, respectively in terms of FDR at$Wr = 1$. Further, the F1 score of the proposed MPCA-ADA model is high, and it is 61%, 55% and 11.1% superior to the existing models like PCA-ADA, LDA-ADA, ICA-ADA, respectively as shown in Fig. 2(i). The MCC of the proposed MPCA-ADA model is high, which is 50% better than PCA-ADA, 75% better than LDA-ADA, 25% better than ICA-ADA at$Wr = 1$, as per Fig. 2(j).

5.3. Algorithmic analysis for test case 2

Fig. 4 reviews the performance of proposed MPCA-ADA classifier over the other methods for test case 2. From Fig. 4(a) it is clear that the proposed MPCA-ADA model is 63%, 52% and 55% superior to the existing

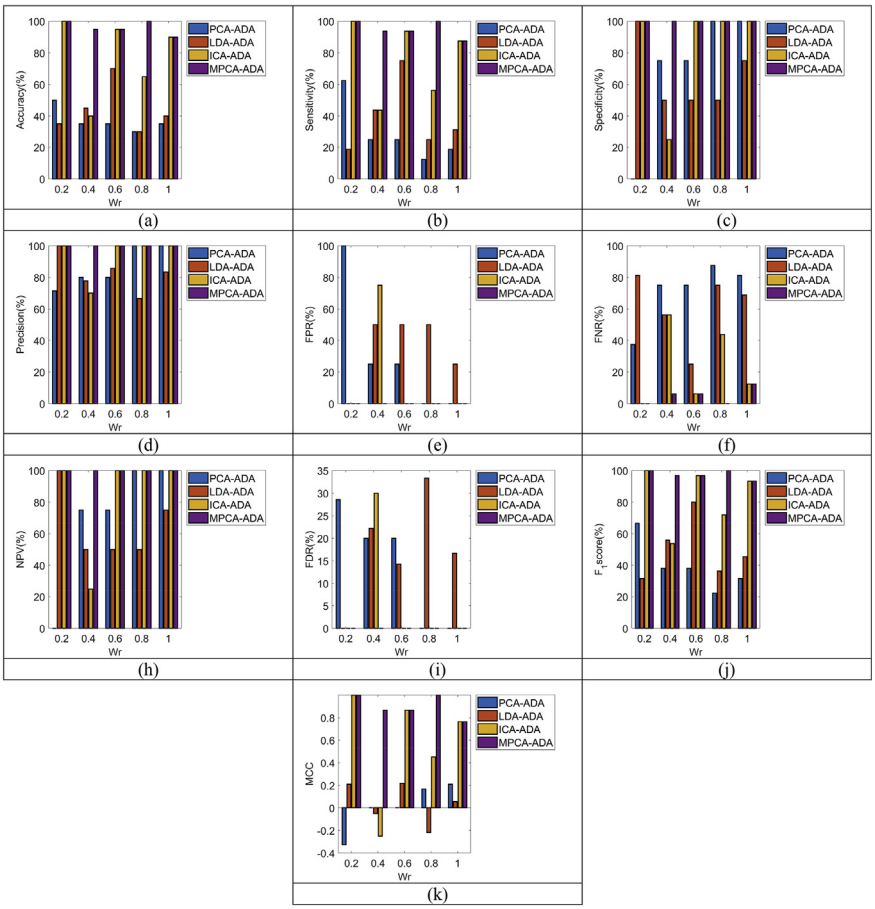

Fig. 4. Algorithmic analysis on the performace of proposed MPCA-ADA over the existing classifier for Test Case 2 in terms of (a) Accuracy (b) Sensitivity (c) Specificity (d)Precision (e) FPR (e) FPR (f) FNR (g) NPV (h) FDR (i) F1- score (j) MCC.

models like PCA-ADA, LDA-ADA and ICA-ADA, respectively at $Wr = 0.2$ in terms of accuracy. The sensitivity of the proposed MPCA-ADA model is 90% better then PCA-ADA, 70% better than LDA-ADA and 40% better than ICA-ADA at $Wr = 0.6$as shown in Fig.4 (b). Then, Fig.4(c) exhibits the specificity of the proposed MPCA-ADA model is 33%, 55% and 80% superior to the traditional models like PCA-ADA, LDA-ADA, ICA-ADA, respectively at $Wr = 0.4$. Then, from$Wr = 0.4$ in Fig. 4(d) and the precision of the proposed model is found to be 25%, 22% and 35% superior to the existing models like PCA-ADA, LDA-ADA, and ICA-ADA, respectively. FPR of MPCA-ADA is 80%, 88%, and 93% better than the existing models like PCA-ADA, LDA-ADA and ICA-ADA, respectively at $Wr = 1$ as shown in Fig. 4(e). Then, from Fig. 3(f), FNR of the proposed MPCA-ADA is found to be 86%, 81%, and 82% better than the traditional models like PCA-ADA, LDA-ADA and ICA-ADA, respectively at $Wr = 0.4$ in terms of FNR. Further, in Fig. 4(g), $Wr = 1$ and NPV is found to be 33.3%, 50%, and 75% better than the traditional models like PCA-ADA, LDA-ADA and ICA-ADA, respectively. In Fig. 4(h), $Wr = 0.4$and the proposed MPCA-ADA is evaluated to be 90%, 91%, and 95% better than the existing models like PCA-ADA, LDA-ADA, ICA-ADA, respectively in terms of FDR. Then, F1 score of the proposed MPCA-ADA model is found to be 61.2%, 40.8%, and 44.8% better than the existing models like PCA-ADA, LDA-ADA, ICA-ADA, respectively, while fixing the $Wr = 0.4$as per Fig. 4(i). Then, from fig. 4(j), $Wr = 0.8$and the MCC values were evaluated to be 80% superior to PCA-ADA and 50% better than ICA-ADA.

5.4. Algorithmic analysis for test case 3

Fig. 5 exhibits the analysis on the performance of proposed MPCA-ADA classifier for test case 3. The accuracy of the proposed MPCA-ADA model is 81%, 35%, and 5% better than the conventional models like PCA-ADA, LDA-ADA and ICA-ADA, respectively at $Wr = 1$as per Fig.5 (a). The sensitivity of the proposed MPCA-ADA model at the $Wr = 0.4$is 40%, 25%, and 60% better than the traditional models like PCA-ADA, LDA-ADA and ICA-ADA, respectively in terms of sensitivity as shown in Fig. 5(b). The enhancement in the specificity of the proposed MPCA-ADA model is evaluated by fixing the $Wr = 1$in fig. 5(c) and the evaluation proved that the proposed MPCA-ADA model is 50% better than PCA-ADA, 51% better than LDA-ADA and 2% better than ICA-ADA, respectively. From Fig. 5(d), the proposed MPCA-ADA model is 15%, 12%, and 1% better than the conventional models like PCA-ADA, LDA-ADA and ICA-ADA at $Wr = 1$in terms of precision. Then, FPR of the proposed MPCA-ADA model is 98% and 96% better than the traditional models like PCA-ADA and LDA-ADA, respectively as shown in Fig. 5(e). From Fig.5 (f), FNR of the proposed MPCA-ADA model $Wr = 1$ is 95%, 93%, and 86.6% better than the traditional models like PCA-ADA, LDA-ADA and ICA-ADA, respectively. Then, at $Wr = 0.8$in Fig. 5(g) and the proposed MPCA-ADA model is 98% better than PCA-ADA and LDA-ADA, respectively in terms of NPV. In Fig. 5 (h), the proposed MPCA-ADA model is 76% and 83% superior to the conventional models like PCA-ADA and LDA-ADA in terms of FDR, at$Wr = 0.2$. Then, the proposed MPCA-ADA model is 35%, 21.5% and 5% superior to the conventional models like PCA-ADA, LDA-ADA and ICA-ADA in terms of F1 score at $Wr = 1$as per Fig. 5(i). Further, Fig.5 (j) manifests that the MCC values of the proposed MPCA-ADA model is 90% superior to PCA-ADA, 85% superior to LDA-ADA and 20% superior to ICA-ADA, respectively at $Wr = 1$.

5.5. Comparative analysis based on classifiers

The proposed ADA-NN classifier is compared with conventional

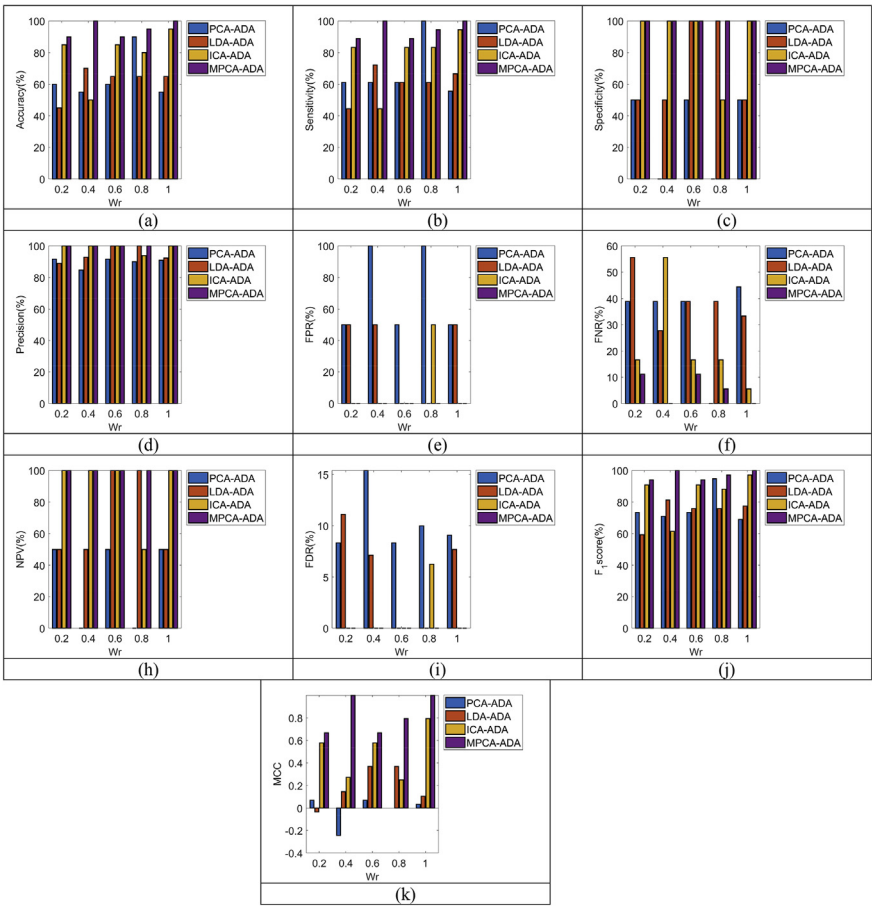

Fig. 5. Algorithmic analysis on the performace of proposed MPCA-ADA over the existing classifier for Test Case 3 in terms of (a) Accuracy (b) Sensitivity (c) Specificity (d)Precision (e) FPR (e) FPR (f) FNR (g) NPV (h) FDR (i) F1- score (j) MCC.

Table 2
Comparative analysis on performance of the proposed classifier over the existing classifier for Test Case 1.

Metrics	Classifiers				
	KNN	SVM	NB	LM-NN	ADA-NN
Accuracy	0.9	0.9	0.9	0.9	0.95
Sensitivity	0.8	0.9	0.9	1	1
Specificity	1	0.9	0.9	0.8	0.9
Precision	1	0.9	0.9	0.83333	0.90909
FPR	0	0.1	0.1	0.2	0.1
FNR	0.2	0.1	0.1	0	0
NPV	1	0.9	0.9	0.8	0.9
FDR	0	0.1	0.1	0.16667	0.090909
F1-Score	0.88889	0.9	0.9	0.90909	0.95238
MCC	0.8165	0.8	0.8	0.8165	0.90453

classifiers such as K-nearest Neighbors (KNN), Support Vector Machine (SVM), Naive Bayes (NB), and LM-NN. Table 2 summarizes the performance analysis of proposed ADA-NN classifier over the other conventional classifiers for test case 1. Here, the accuracy of the proposed model is 5.55% better than KNN, SVM, NB and LM-NN. The sensitivity of the proposed model is 25% better than KNN, 11.11% better than SVM and NB. Further, the specificity of the proposed model is 12.5% better than LM-NN. The FNR of the proposed ADA model is 0.5% better than NN. Moreover, the MCC of the proposed model is 10.78%, 85.55%, 85.55%, and 10.78% superior to than KNN, SVM, NB and LM-NN. Table 3 analyses the performance of proposed ADA-NN classifier over the other methods for test case 2. From table it is clear that the proposed ADA model is 11.76% and 52% superior to the existing models like KNN and SVM in terms of accuracy. The sensitivity of the proposed ADA-NN model is

Table 3
Comparative analysis on performance of the proposed classifier over the existing classifier for Test Case 2.

Metrics	Classifiers				
	KNN	SVM	NB	LM-NN	ADA-NN
Accuracy	0.85	0.85	0.95	0.8	0.95
Sensitivity	0.8125	0.8125	0.9375	0.75	1
Specificity	1	1	1	1	0.75
Precision	1	1	1	1	0.9411
FPR	0	0	0	0	0.25
FNR	0.1875	0.1875	0.0625	0.25	0
NPV	1	1	1	1	0.75
FDR	0	0	0	0	0.0588
F1-Score	0.8965	0.8965	0.967	0.85714	0.9697
MCC	0.6813	0.6813	0.8660	0.61237	0.84017

Table 4
Comparative analysis on performance of the proposed classifier over the existing classifier for Test Case 3.

Metrics	Classifiers				
	KNN	SVM	NB	LM-NN	ADA-NN
Accuracy	0.94444	0.888	0.888	0.944	0.944
Sensitivity	1	1	1	1	1
Specificity	1	1	1	1	1
Precision	0	0	0	0	0
FPR	0.0555	0.11111	0.111	0.0555	0.0555
FNR	1	1	1	1	1
NPV	0	0	0	0	0
FDR	0.971	0.941	0.941	0.971	0.971
F1-score	0.793	0.666	0.666	0.793	0.793
MCC	0.95	0.9	0.9	0.95	0.95

23.07% better than KNN and SVM, 23.07% better than NB and 33.33% better, the F1-Score of the proposed model is 1% better than LM-NN. The FNR of the proposed model is 1% better than KNN, SVM, NB and LM-NN. Moreover, it is 86% better than KNN and SVM. In addition the MCC of the proposed model shows 13.06% and 10.78% better than NB and LM-NN classifier. Table 4 exhibits the analysis on the performance of proposed ADA-NN classifier for test case 3. The accuracy of the proposed model is 6.30% better than SVM and NB classifier. The FDR of the proposed model is 3.18% better than SVM and NB classifier .

6. Conclusion

This paper has developed an algorithmic analysis on novel caries detection model in order to have an accurate detection in the tooth cavities. The proposed caries detection model was divided into two phases: feature extraction and classification. The feature extraction was done based on MPCA, and the classification was done using NN classifier. The feature extraction and classification were done on image after pre-processing with contrast enhancement, Gray threshold, and active contour. The extracted features were multiplied with the weighting factor, and then the Nonlinear Programming Optimization was employed with an intention of maximizing the distance between the resultant feature outputs.The training of NN classifier was accomplished using ADA algorithm. Finally, an algorithmic analysis was carried for MPCA –ADA over the conventional classifier models like PCA-ADA, LDA-ADA and ICA-ADA in terms of Accuracy, Sensitivity, Specificity, Precision, FPR, FNR, NPV, FDR, F1Score and MCC for Test case1, Test case2, test case 3.

Declarations

Author contribution statement

Shashikant Patil: Conceived and designed the experiments; Performed the experiments; Analyzed and interpreted the data; Contributed reagents, materials, analysis tools or data; Wrote the paper.

Vaishali Kulkarni: Conceived and designed the experiments; Contributed reagents, materials, analysis tools or data; Wrote the paper.

Archana Bhise: Conceived and designed the experiments; Analyzed and interpreted the data; Wrote the paper.

Funding statement

This research did not receive any specific grant from funding agencies in the public, commercial, or not-for-profit sectors.

Competing interest statement

The authors declare no conflict of interest.

Additional information

No additional information is available for this paper.

References

[1] K. Angelino, D.A. Edlund, P. Shah, Near-Infrared imaging for detecting caries and structural deformities in teeth, IEEE J. Transl. Eng. Health. Med. 5 (2017) 1–7.

[2] S. Keem, M. Elbaum, Wavelet representations for monitoring changes in teeth imaged with digital imaging fiber-optic transillumination, IEEE Trans. Med. Imag. 16 (5) (Oct. 2007) 653–663.

[3] Abdolvahab Ehsani Rad, Mohd Shafry Mohd Rahim, Hoshang Kolivand, Alireza Norouzi, Automatic computer-aided caries detection from dental x-ray images using intelligent level set, Multimed. Tool. Appl. 77 (21) (November 2018) 28843–28862.

[4] Joonhyang Choi, Hyunjun Eun, Changick Kim, Boosting proximal dental caries detection via combination of variational methods and convolutional neural network, J. Signal Process. Syst. 90 (1) (January 2018) 87–97.

[5] Suwadee Kositbowornchai, Sanphet Siriteptawee, Supattra Plermkamon, Sujin Bureerat, Danaipong Chetchotsak, An artificial neural network for detection of simulated dental caries, J. Comput. Assist. Radiol.Surg. 1 (2) (August 2006) 91–96.

[6] R.C. Lee, M. Staninec, O. Le, D. Fried, Infrared methods for assessment of the activity of natural enamel caries lesions, IEEE J. Sel. Top. Quantum Electron. 22 (3) (May-June 2016) 102–110.

[7] K. Angelino, D.A. Edlund, P. Shah, Near-infrared imaging for detecting caries and structural deformities in teeth, IEEE J. Transl. Eng. Health Med. 5 (2017) 1–7.

[8] H. Kang, J.J. Jiao, C. Lee, M.H. Le, C.L. Darling, D. Fried, Nondestructive assessment of early tooth demineralization using cross-polarization optical coherence tomography, IEEE J. Sel. Top. Quantum Electron. 16 (4) (July-Aug. 2010) 870–876.

[9] Eun-Soo Kim, Eun-Song Lee, Si-Mook Kang, Eun-Ha Jung, Baek-Il Kim, A new screening method to detect proximal dental caries using fluorescence imaging, Photodiagn. Photodyn. Ther. 20 (December 2017) 257–262.

[10] Maria Eliza Soares, Maria Letícia Ramos-Jorge, Bruna Mota de Alencar, Simone Gomes Oliveira, Joana Ramos-Jorge, Influence of masticatory function, dental caries and socioeconomic status on the body mass index of preschool children, Arch. Oral Biol. 81 (September 2017) 69–73.

[11] Jie Deng, Leanne Jackson, Joel B. Epstein, Cesar A. Migliorati, Barbara A. Murphy, Dental demineralization and caries in patients with head and neck cancer, Oral Oncol. 51 (9) (September 2015) 824–831.

[12] K.W. Neuhaus, F. Jost, P. Perrin, A. Lussi, Impact of different magnification levels on visual caries detection with ICDAS, J. Dent. 43 (12) (December 2015) 1559–1564.

[13] Sug-Joon Ahn, Young-Doo Song, Su-Jung Mah, Eun-Jung Cho, Joong-Ki Kook, Determination of optimal concentration of deglycyrrhizinated licorice root extract for preventing dental caries using a bacterial model system, J. Dent. Sci. 9 (3) (September 2014) 214–220.

[14] Massimo Costalonga, Mark C. Herzberg, The oral microbiome and the immunobiology of periodontal disease and caries, Immunology 162 (2) (December 2014) 22–38.

[15] Peter Usenik, Miran Bürmen, Aleš Fidler, Franjo Pernuš, Boštjan Likar, Near-infrared hyperspectral imaging of water evaporation dynamics for early detection of incipient caries, J. Dent. 42 (10) (October 2014) 1242–1247.

[16] Emily Ming Jiang, Edward Chin Man Lo, Chun Hung Chu, May Chun Mei Wong, Prevention of early childhood caries (ECC) through parental toothbrushing training and fluoride varnish application: a 24-month randomized controlled trial, J. Dent. 42 (12) (December 2014) 1543–1550.

[17] M.R. Alammari, P.W. Smith, E. de Josselin de Jong, S.M. Higham, Quantitative light-induced fluorescence (QLF): a tool for early occlusal dental caries detection and supporting decision making in vivo, J. Dent. 41 (2) (February 2013) 127–132.

[18] Kenneth Markowitz, Dalia Rosenfeld, Daniel Peikes, Gerald Guzy, Glenn Rosivack, Effect of pit and fissure sealants on caries detection by a fluorescent camera system, J. Dent. 41 (7) (July 2013) 590–599.

[19] Donald R. Schwass, Jonathan W. Leichter, David G. Purton, Michael V. Swain, Evaluating the efficiency of caries removal using an Er:YAG laser driven by fluorescence feedback control, Arch. Oral Biol. 58 (6) (June 2013) 603–610.

[20] N.C. Santos, S. Jamelli, L. Costa, C. Baracho Filho, E. Sarinho, Assessing caries, dental plaque and salivary flow in asthmatic adolescents using inhaled corticosteroids, Allergol. Immunopathol. 40 (4) (July–August 2012) 220–224.

[21] A. Alsam, I. Farup, H.J. Rivertz, Iterative sharpening for image contrast enhancement, in: Colour and Visual Computing Symposium (CVCS), 2015, pp. 1–4. Gjovik.

[22] Hetal J. Vala, Astha baxi, A review on Otsu image segmentation algorithm, Int. J. Adv. Res. Comput. Eng.& Technol. (IJARCET) 2 (2) (2013).

[23] Haiping Lu, Konstantinos N. (Kostas) Plataniotis, Anastasios N. Venetsanopoulos, MPCA: multilinear principal component analysis of tensor objects, IEEE Trans. Neural Netw. 19 (1) (2008).

[24] Mohammad Jafari, Mohammad Hossein Bayati Chaleshtari, Using dragonfly algorithm for optimization of orthotropic infinite plates with a quasi-triangular cut-out, Eur. J. Mech. A Solid. 66 (2017) 1–14.

[25] JürgenSchmidhuber, Deep learning in neural networks: an overview, Neural Network. 61 (2015) 85–117.

[26] G.Y. Zhang, G.Z. Liu, H. Zhu, B. Qiu, Ore image thresholding using bi-neighbourhood Otsu's approach, Electronics Letters 46 (25) (9 December 2010) 1666–1668. ISSN: 0013-5194 INSPEC Accession Number: 11775377.

[27] Kuo-Huang Lin, Bin-Da Liu, A gray system modeling approach to the prediction of calibration intervals, IEEE Trans. Instrum. Meas. 54 (1) (Feb. 2005) 297–304.

[28] Mamta Mittal, Lalit Mohan Goyal, D Jude Hemanth, Jasleen Kaur Sethi, Clustering Approaches for High-Dimensional Databases: A Review, WIREs Data Mining Knowl Discov (2019). John Wiley & Sons.

[29] Mamta Mittal, Rajendra Kumar Sharma, Varinder Pal Singh, Performance evaluation of threshold-based and k-means clustering algorithms using Iris dataset, recent patents on engineering published by, Bentham Science (2018).

[30] B. Kaur, M. Sharma, M. Mittal, A. Verma, L.M. Goyal, D.J. Hemanth, An improved salient object detection algorithm combining background and foreground connectivity for brain image analysis, Comput. Electr. Eng. 71 (2018) 692–703.